machines

MDPI

Article

Numerical Investigation on the Combustion and Emission Characteristics of Diesel Engine with Flexible Fuel Injection

Qihao Mei [1], Intarat Naruemon [2], Long Liu [1,*], Yue Wu [1] and Xiuzhen Ma [1]

[1] College of Power and Energy Engineering, Harbin Engineering University, Harbin 150001, China
[2] Mechanical Engineering Program, Faculty of Engineering, Thaksin University, Pa Payam 93110, Thailand
* Correspondence: liulong@hrbeu.edu.cn; Tel.: +86-451-8256-8316

Abstract: As the main engineering power plant, diesel engines are irreplaceable in the future. However, the stringent emission regulations impose many tough requirements to their developments. Recently, flexible fuel injection strategy has been recognized as an effective technology in creating an advanced spray and mixture formation and improving combustion efficiency indirectly. However, the detailed combustion and emission behaviors under flexible fuel injection are still unknown. Therefore, this paper aims to investigate the combustion and emission characteristics under flexible fuel injection and explore an optimal injection strategy for high-efficiency combustion. A numerical simulation method is conducted by coupling the large-eddy simulation (LES) model and the SAGE combustion model. Then, the spray mixing, combustion flame propagation and emissions formation under various multiple-injection strategies are investigated. Results reveal that initial an ultrahigh injection pressure has a significant influence on the spray's axial penetration while dwell time mainly affects the spray's radial expansion. Under an initial ultrahigh injection pressure, the turbulence kinetic energy (TKE) becomes larger, and the vortex motions are stronger, contributing to a better spray turbulent mixing. Meanwhile, a snatchier flame structure with a favorable level of equivalence ratio and a homogeneous temperature distribution is obtained. In this way, the peak heat release rate (HRR) could increase by 46.7% with a 16.7% reduction in soot formation and a 31.4% reduction in NO_x formation.

Keywords: diesel engine; flexible fuel injection; spray and mixture formation; high-efficiency combustion; large eddy simulation

Citation: Mei, Q.; Naruemon, I.; Liu, L.; Wu, Y.; Ma, X. Numerical Investigation on the Combustion and Emission Characteristics of Diesel Engine with Flexible Fuel Injection. *Machines* **2023**, *11*, 120. https://doi.org/10.3390/machines11010120

Academic Editor: Ahmed Abu-Siada

Received: 3 December 2022
Revised: 28 December 2022
Accepted: 10 January 2023
Published: 16 January 2023

1. Introduction

Benefiting from a high thermal efficiency, high torque and high power density, diesel engines will still be an irreplaceable main power plant in future engineering field [1,2]. However, the accompanied emission problems of NO_x and CO_2 have been deep-rooted in diesel engines [3–5]. With the exhaust emission regulation increasingly stringent [6,7], diesel engines are facing more and more huge challenges in practical engineering applications. Intuitively, exploring the advanced combustion strategies is an imperative and effective way to reduce the emissions and improve the thermal efficiency of diesel engines. Moreover, many important improvements have been achieved, such as the technologies of premixed charge combustion ignition (PCCI) [8], low-temperature combustion (LTC) [9] and exhaust gas recirculation (EGR) [5,10], which have improved the emission characteristics and promoted the engine efficiency to a certain extent. However, faced with the increasingly stringent emission regulations, these technologies gradually hit a bottleneck for the further optimization of diesel engine performance. Recently, more and more attention has been paid to the advanced spray and mixture formation in engines, because it plays an important role in controlling a high-efficiency combustion and shows a high degree of flexibility and controllability for wide operating condition. Fuel injection is a dominating factor that affects the spray and mixture formation. The rapid innovation of fuel injection technologies

has greatly promoted the development of advanced injection strategies [11,12], such as an ultrahigh injection pressure, injection rate shaping and the multiple-injection strategy, which have a significant importance on the spray mixing and combustion process.

Injection pressure determines the jet momentum out of the nozzle orifice and directly influences the spray mixing, penetrating and turbulent diffusing process. Many studies have shown that increasing the injection pressure could sharply accelerate the fuel–air mixing process, thereby improving the combustion efficiency while reducing the emission of diesel engines simultaneously [13,14]. Therefore, the injection pressure has been developing towards a higher level. Currently, an ultrahigh injection pressure of 500 MPa has been reached [15]. It was found that the shock waves were created inside the chamber, which would disrupt the spray flow, causing it to mix better. Meanwhile, the increased momentum enhanced mixing, further improving the combustion characteristic. Understanding the detailed spray and mixture formation process is fairly important to adjust the fuel injection strategy for an optimal combustion process. However, the current research about the effect of ultrahigh injection pressure on spray mixing and combustion process still stays in the apparent characteristic parameters, and the deeply detailed evolution processes such as the fuel–air interaction, flame propagation and combustion products formation under ultrahigh injection pressure are not well understand.

The rapid innovations of piezoelectric injector, in terms of fast needle response time and high controllability [11,12], have greatly promoted the development of injection rate reshaping and multiple-injection technologies. In our previous studies [16,17], we found that varying injection rates had a great importance on the spray characteristics, such as penetration, entrainment rate, turbulence kinetic energy and equivalence ratio. Meanwhile, some studies also demonstrated that injection rate shape was closely related with the combustion characteristics. For example, Macian et al. [12] proved that adjusting the injection rate could control the fuel amount involved in the premix combustion, which affected the NO_x production and the engine noise. Boggavarapu et al. [18] and Ramirez et al. [19] revealed that increasing the injection rate slowly at the initial injection could reduce the NO_x and the indicated mean effective pressure, but with a negative effect on the soot emissions. Then, Mohan et al. [20] and Tay et al. [21] demonstrated that boot, ramp and triangular injection rate shapes had a great influence on the combustion characteristics of diesel engines, respectively. The proposal of multiple-injection further added the complexities of the fluid flow in the cylinder of diesel engines, but also enriched the flexibilities of advanced fuel injection strategies. Several recent achievements have discovered that multiple injection strategies benefit a lot to the spray mixing and combustion process. For instance, Skeen et al. [22] found that the high-temperature entrainment gases and intermediate species from the first injection contributed to a shorter ignition delay for the second injection. It was because the increased pressure and local temperature created a good ignition condition for the second injection [23]. Similarly, Cung et al. [24] and Moiz et al. [25] concluded that multiple-injection could enhance the interaction between the previously injected jet flame and the impending cold spray, which would influence the ignition process and the emission characteristic of the latter injection. In addition, Zheng et al. [26] noted that increasing the dwell time would cause the combustion region to move far away from the second injection, resulting in an increased surrounding oxygen entrainment into the flame region and finally, reduced soot emissions. Overall, these studies fully reflected the significant importance of multiple-injection on the spray combustion characteristics, but the subinjection was limited to a constant injection rate shape with a conventional injection pressure. Undoubtedly, the combination of injection rate reshaping and multiple-injection strategies must provide even more advantages and is well worth deeply studying. Therefore, we recently carried out an in-depth study about the effect of multiple-injection with different injection patterns under ultrahigh injection pressure on the diesel spray mixing process [27]. It was found that the dwell time of multiple-injection and the inverse injection pressure both greatly affected the turbulence structure. Meanwhile, an optimal injection strategy was obtained to achieve the best spray and mixture formation. This finding could absolutely provide an effective and

valuable guidance for the injection strategy design to improve the fuel–air mixing process of diesel engines under various engineering application conditions. However, the effect of this kind of split injection on the combustion and emission characteristics under ultrahigh injection pressure is not known clearly and remains to be further studied.

Diesel spray combustion is an extremely complicated process, involving many details such as highly nonlinear chemical kinetics, small-scale velocity, scalar mixing, turbulence–chemistry interactions, compressibility effects and variable inertia effects. Unfortunately, limited by the current visualizing and testing technologies, the detailed diesel spray combustion process is difficult to capture, especially for the highly integrated diesel engines in practical engineering applications. Therefore, a computational fluid dynamics (CFD) simulation is an effective alternative method for more intensive study. Meanwhile, it could also greatly conserve human, physical and financial resources, and provide a fast yet flexible prediction tool in engineering applications. In diesel spray combustion simulations, the unsteady Reynolds averaged Navier–Stokes (URANS) technique and large-eddy simulation (LES) are two common methods. However, the URANS technique employs a filtering in time to derive the governing conservation equations for the mean state, so some local instabilities in the flow cannot be simulated. Instead, the LES has historically employed spatial filtering to split the field variables into time-dependent resolved-scale and subgrid-scale components, so the whole-scale turbulent features can be well simulated. Because of this, Rostampour et al. [28] simulated a more accurate spray contour shape by using the LES model, and Nemati et al. [29] captured a more accurate heat release result in the LES case. Recently, Salehi et al. [30] and Wen et al. [31] successively carried out LES investigations of the spray and flame characteristics under various injection pressures and multi-injection, respectively; both obtained an accurate and satisfactory result. For a better description of the combustion behavior, the SAGE combustion model is a fine choice. It contains the detailed chemical kinetic solutions [32] and can directly combine the chemical reaction rate with a chemical mechanism using a series of fundamental reactions to describe the overall reaction. Sun et al. [33] found that using the SAGE combustion model could obtain a more accurate simulation result of the in-cylinder maximum combustion pressure than other models. While with the help of an LES and detailed chemical kinetics, Gong et al. [34] investigated the stabilization mechanisms and the autoignition characteristic of an n-dodecane spray flame under the engine conditions. They found that the two-step ignition behavior was well predicted; meanwhile, the stability of the flame lift-off resulted from the competition of the autoignition and flame propagation spread. These studies fully demonstrated the incomparable advantages of the LES model and SAGE combustion model in simulating the turbulent flow involving heterogeneous chemically reacting multiphase mixtures in diesel engines. In our previous paper [27], it was found that the varying injection rate would contribute to a much more chaotic vortex motion and a snatchier and more dispersive spray contour, due to the unsteady fluid momentum supply. Moreover, the overlapping flow and backflow movements occur frequently because of the rapid change of injection pressure. Since the vortex greatly controls the transports of species, momentum and energy, the turbulent flow characteristic under the varying injection rate makes the spray equivalence ratio distribution become highly heterogeneous, which certainly influences the following combustion and emission characteristics. For example, the soot appears mainly in the rich fuel area while the NO_x generates mainly in the high-temperature region. Particularly, when coupling the varying injection rate with an ultrahigh injection pressure and the multiple-injection strategy, the strengthened TKE and shock wave from the ultrahigh injection pressure further disturb and deform the turbulent vortex structure, while the enhanced entrainment wave from the multiple-injection strategy splits the turbulent vortex and change its motion simultaneously. In this way, the turbulent spray becomes much more heterogeneous, and the interaction of turbulent mixing, vortex motion and flame–flame diffusion becomes extremely complicated. However, these processes occur at time scales of micro- or nanoseconds with entirely different scales, creating stringent constraints for an experimentally study. Fortunately, using the LES model could obtain a thoroughly detailed

structure of the complicated turbulent flow, both in large-scale and small-scale observations. Moreover, the unsteady vortex motion and interaction could be vividly and accurately captured, providing a detailed distribution information of species concentration with a high degree of fidelity. Then, coupling with the SAGE combustion model, the local transient combustion processes in the heterogeneous turbulent flame could be described precisely and in detail, better reflecting the spray flame behavior in practical diesel engines. By this means, we could gain more insights into the in-cylinder phenomena under the varying injection rate with an ultrahigh injection pressure and the multiple-injection strategy, then design an optimal injection strategy to avoid abnormal combustions. Obviously, it will play a vitally important role in the improvement of combustion and emission characteristics in engineering applications. However, there has not yet been a detailed and comprehensive study of this aspect, and gaps remained to be filled.

In a continuation with our previous effort about the effect of a flexible fuel injection strategy on the diesel spray and mixture formation, this paper mainly aims to investigate the combustion and emission characteristics of a diesel engine under a flexible fuel injection strategy with an ultrahigh injection pressure and explore an optimal injection strategy for engineering applications to cope with the increasingly serious emission problems. In this study, the popular CFD method, LES, is coupled with the SAGE combustion model to simulate the diesel spray combustion process. In addition, the experimental data of Spray A from the Engine Combustion Network (ECN) [35], which is a worldwide group of institutions establishing an internet library of well-documented combustion vessels experiments that are appropriate for CFD model validation and the advancement of scientific understanding of combustion at engine-relevant conditions, are used for the model validation. Finally, the numerical results of combustion and emission characteristics under various injection strategies are comprehensively and thoroughly compared and discussed.

2. Numerical Setup

In this paper, the investigation of the diesel spray combustion behavior was conducted by the three-dimensional (3D) CFD software package of CONVERGE 2.4, and the popular Lagrangian-parcel Eulerian-fluid method [36] was implemented for the simulation analysis of the diesel spray mixing and combustion process. Submodels including the spray injection model, atomization model, turbulence model, droplet collision and integration model were considered. Meanwhile, the pressure and the speed were coupled together in the simulation using the algorithm of Pressure-Implicit with Splitting of Operators (PISO). Then, the Kelvin–Helmholtz (KH) and Rayleigh–Taylor (RT) models were used to predict the droplet breakup process. Moreover, the droplet collisions were created with the no-time-counter algorithm (NTC), and the Frossling correlation model was used to describe the droplet evaporation process. As for the turbulence model, the dynamic structure in conjunction with the LES was considered. Finally, the popular SAGE model was used to simulate the detailed combustion process. All the submodels used in this study are listed in Table 1.

Table 1. Numerical setup.

Modeling Tool	Converge
Spray models	
Drop evaporation model	Frossling model
Collision model	NTC collision
Collision outcome	O'Rourke collision outcomes
Drop drag model	Dynamic drop drag
Breakup	KH-RT model
Turbulence model	LES, Dynamic Structure
Combustion model	SAGE

The 3D CFD simulation of the spray combustion process was conducted on a constant-volume combustion chamber (CVCC), as shown in Figure 1, which is referenced in the experiments of Spray A from ECN website [35]. The CVCC had a diameter of 105 mm and a length of 105 mm, with an injector mounted on the top center of the chamber. The experimental conditions of Spray A from the ECN website [35] were used as the boundary conditions of the numerical study in this study. In addition, this study followed the same grid settings as in our previous work [27], using the adaptive mesh refinement and the fixed embedding to achieve a finer mesh in the critical area, in order to achieve a good accuracy at reasonable computational costs. Based on the independent analysis of the mesh, the finest cell size setting of 125 µm was selected. The finest cell size (125 µm) covered a 15 mm gap between the nozzle and downstream to ensure a sufficient resolution at the mixing density location. Moreover, the vapor penetration region rest was set up with a cell size of 250 µm. The computational domain of the studied LES was separated into a mesh with different levels of cell sizes. The adjustment layer was specified with R1, R2, R3, and R4 as shown in Figure 1, which corresponded to cell sizes of 4000 µm, 2000 µm, 250 µm and 125µm, respectively. The separate domains corresponded to the volume of the experimental combustion vessel at the Sandia National Laboratories comprising approximately 1.9 million hexahedral cells. Further grid settings details can be found in our previous study [27].

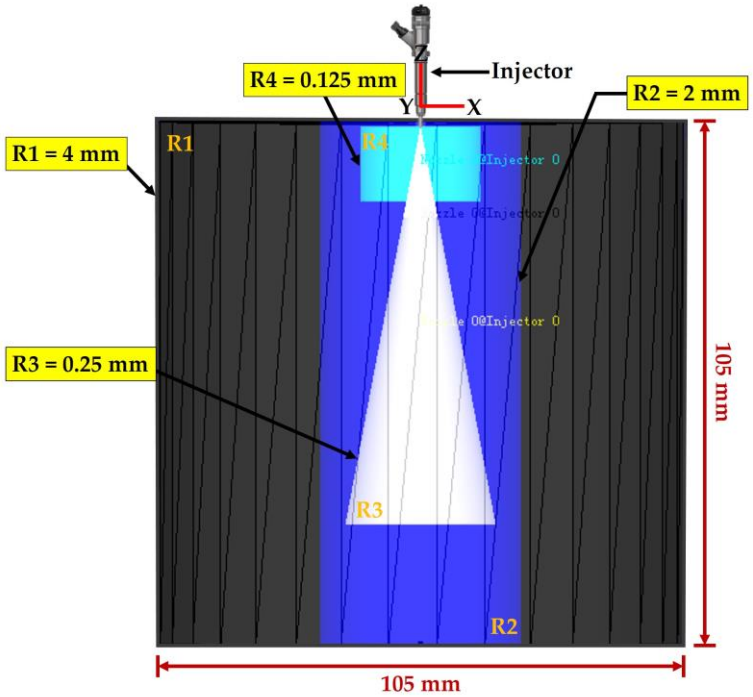

Figure 1. Geometric structure of CVCC and computational domain.

2.1. Spray Breakup Modeling

This paper used the KH-RT model to simulate the droplet breakup process. The KH-RT model is a hybrid method consisting of the KH wave model and RT, the instability of a normal acceleration to the droplet surface. The KH mechanism considers droplets to be liquid jets that have been stripped after being injected into the gas environment, while the RT mechanism is driven by changes in density in the normal direction of the liquid–gas interface. The KH model based on the disruptive growth rate Ω_{KH} and the wavelength Λ_{KH} that corresponds to the fastest Ω_{KH} has a characteristic breakup time τ_{KH}, which can be defined as follows:

$$\tau_{KH} = \frac{3.276 B_1 r}{\Omega_{KH} \Lambda_{KH}} \quad (1)$$

where r is the radius of the initial droplets and B_1 is a KH model constant. When considering the RT model by assuming that there is a linear disturbance growth, the growth rate of Ω_{RT} and Λ_{RT} of the wavelength can be determined. The RT breakup time τ_{RT} is given by the multiplicative inverse of the growth rate:

$$\tau_{RT} = C_\tau \frac{1}{\Omega_{RT}} \tag{2}$$

where C_τ is the correction factor to delay the breakup under certain conditions.

2.2. Turbulence Modeling

As mentioned above, the LES model is best-suited for unsteady turbulent conditions in engine-scale simulations. The turbulent gas flow is explained by using compressible Navier–Stokes equations in the Eulerian framework. Favre filtered LES formulations for the conservation of mass, species mass fractions, momentum and energy equations are the followings

$$\frac{\partial \overline{\rho}}{\partial t} + \frac{\partial \overline{\rho}\widetilde{u_i}}{\partial x_i} = \overline{S}_\rho \tag{3}$$

$$\frac{\partial (\overline{\rho}\widetilde{u_i})}{\partial t} + \frac{\partial \left(\overline{\rho}\widetilde{u_i}\widetilde{u_j}\right)}{\partial x_i} = \frac{\partial}{\partial x_j}\left(-\overline{p}\delta_{ij} + \overline{\rho}\widetilde{u_i}\widetilde{u_j} - \overline{\rho}\widetilde{u_i u_j} + \overline{\tau}_{ij}\right) + \overline{S}_{u_i} \tag{4}$$

$$\frac{\partial \left(\overline{\rho}\widetilde{Y_k}\right)}{\partial t} + \frac{\partial (\overline{\rho}\widetilde{u_i}\widetilde{u_k})}{\partial x_i} = \frac{\partial}{\partial x_j}\left(\overline{\rho}\widetilde{u_i} - \overline{\rho}\widetilde{u_i Y_k} + \overline{\rho}\widetilde{D}\frac{\partial \widetilde{Y_k}}{\partial x_i}\right) + \overline{S}_{Y_k} \tag{5}$$

$$\frac{\partial \left(\overline{\rho}\widetilde{h_t}\right)}{\partial t} + \frac{\partial \left(\overline{\rho}\widetilde{u_j}\widetilde{h_t}\right)}{\partial x_j} = \frac{\partial \overline{p}}{\partial t} + \frac{\partial}{\partial x_j}\left(\overline{\rho}\widetilde{u_j}\widetilde{h_s} - \overline{\rho}\widetilde{u_i h_s} + \overline{\mu}\frac{\partial \widetilde{h_s}}{\partial x_j}\right) + \overline{S}_h \tag{6}$$

where ρ, u_i, p, Y_k, h_s and $\overline{\tau}_{ij}$ represent the density, velocity component in the x_i direction, pressure, chemical species k mass fraction, sensible enthalpy and conventional viscous stress tensor assuming Stokes' hypothesis for a isotropic Newtonian fluid, respectively. The overbar and tilde (~) are filter operators that represent the mean values of all unweighted and density-weighted ensemble averages, respectively. The unity Schmidt number is assumed for all species, so the mass diffusivity $D = \mu/\rho$, in which μ means the viscosity diffusion rate of the gas mixture. The total enthalpy h_t refers to the summation of h_s and the specific kinetic energy. The filtered source terms $\overline{S}_\rho$, $\overline{S}_{u_i}$, $\overline{S}_{Y_k}$ and $\overline{S}_h$ correspond to the coupling between the liquid and gas phases in terms of mass, momentum, species and energy, respectively.

The Eulerian source terms $\overline{S}_\rho$ and $\overline{S}_{Y_k}$ are derived from Equations (3) and (5) calculated from the droplet evaporation model utilizing the ideal gas assumption. The momentum source term $\overline{S}_u$ (Equation (4)) is estimated from the drag force of the sphere. The energy source term $\overline{S}_h$ (Equation (6)) is based on the Ranz–Marshall correlation for heat transfer. In Equation (6), the total enthalpy is expressed as the sum of the absolute enthalpy and specific kinetic energy, that is, $\overline{h}_t = \widetilde{h} + \frac{\widetilde{u_i}\widetilde{u_i}}{2}$. The viscous stress tensor is defined as

$$\overline{\tau}_{ij} = \overline{\mu}\left(\frac{\partial \widetilde{u_i}}{\partial x_j} + \frac{\partial \widetilde{u_j}}{\partial x_i} - \frac{2}{3}\frac{\partial \widetilde{u_k}}{\partial x_k}\delta_{ij}\right) \tag{7}$$

where μ is the dynamic viscosity, and the conditions source terms $\overline{S}_\rho$, $\overline{S}_{u_i}$ and $\overline{S}_h$ allow the connection between liquid and gas phases in terms of mass, momentum and energy. The mathematical closure for a system of equations is produced by the filtered ideal gas law and state thermal equation.

2.3. Combustion Modeling

Detailed chemical kinetic mechanisms are important to accurately model the transient, multidimensional chemically reacting flow systems. In this study, the SAGE model that incorporates into the CFD software was used to solve the mass and energy equations using detailed chemistry mechanisms, with the LES model to find out the optimal injection rate for the spray and combustion of diesel engines. In the SAGE model, the forward rate coefficient k_{fr} is represented by the Arrhenius form:

$$k_{fr} = A_r T^{b_r} e^{-\frac{E_r}{R_u T}} \tag{8}$$

where A_r is the factor of the pre-exponential, b_r is the temperature exponent, E_r is the activation energy and R_u is the constant of universal gas. Moreover, the reverse rate coefficient k_{rr} can also be specified in an analogous fashion, calculated from the equilibrium coefficient K_{cr}

$$k_{rr} = \frac{k_{fr}}{K_{cr}} \tag{9}$$

$$K_{cr} = K_{pr}\left(\frac{p_{atm}}{RT}\right)^{\sum_{m=1}^{M} v_{mr}} \tag{10}$$

where p_{atm} is the atmospheric pressure and R is the constant of gas. The equilibrium constant K_{pr} is obtained by:

$$K_{pr} = \exp\left(\frac{\Delta S_r^0}{R} - \frac{\Delta H_r^0}{RT}\right) \tag{11}$$

where Δ is the change that occurs when passing completely from reactants to products in the r^{th} reaction,

$$\frac{\Delta S_r^0}{R} = \sum_{m=1}^{M} v_{mr} \frac{S_m^0}{R} \tag{12}$$

$$\frac{\Delta H_r^0}{RT} = \sum_{m=1}^{M} v_{mr} \frac{H_m^0}{RT} \tag{13}$$

where S is the entropy and H is the enthalpy.

The mass and energy conservation governing the equations for a given computational cell are:

$$\frac{d[X_m]}{dt} = \dot{\omega}_m \tag{14}$$

$$\frac{dT}{dt} = \frac{V\frac{dp}{dt} - \sum_m \left(\overline{h}_m \dot{\omega}_m\right)}{\sum_m \left([X_m]\overline{c}_{p,m}\right)} \tag{15}$$

where $\dot{\omega}_m$ is determined by Equation (9), $\overline{h}_m$ is the molar specific enthalpy of species m and $\overline{c}_{p,m}$ is the molar constant-pressure specific heat of species m.

The above equations were solved at each of the CONVERGE computational time-step and we appropriately updated the species. This study used the n-heptane (C7H16) mechanism, a reduced mechanism developed by the Lawrence Livermore National Laboratory (LLNL, Livermore, CA, USA) [37] containing 42 species and 168 reactions.

3. Results and Discussion

3.1. Model Validation

To calibrate the model accuracy and reliability when predicting the diesel spray combustion behavior, the experimental data of Spray A from ECN [35] were used in this study. Table 2 shows the injection conditions and the ambient conditions.

Table 2. Operating conditions of Spray A from the ECN website [35].

Parameters	Case 1	Case 2
Fuel	n-dodecane	n-dodecane
Nominal nozzle diameter (μm)	84	89
Injection pressure (MPa)	150	150
Injection duration (ms)	1.54	1.60
Ambient temperature (K)	900	900
Ambient density (kg/m^3)	22.8	22.8
Molar concentration of O_2 (%)	15	15

Figure 2 shows the simulated evolution process of the spray combustion flame under different cases. In Figure 2a, obviously, the simulation results of the liquid spray penetration length and the lift-off length approached closely those of the experimental data. At t = 0.9 ms, the whole spray flame profile was gradually formed, and there was not much difference between the simulated spray flame and the experimental image in axial length and radial width. More importantly, similar to the separated layer in the zone with the blue line of the experimental image, the simulation results also obtained a clear flame temperature distribution and detailed vortex structures. At t = 1.2 ms, the separated layer in the zone with the blue line of the experimental image became more obvious, and this change was also dynamically captured by the simulation. Compared with the experimental image, the simulated spray flame was only 8% shorter in axial length and 15% narrower in radial width. At t = 1.8 ms, the fuel was completely evaporated, and the liquid spray penetration length had disappeared both in the experimental image and simulated spray flame. Meanwhile, the flame recession phenomenon in the experimental image was also clearly captured by the simulation. Although the simulated flame length was around 14% shorter than the experimental one, there was no big difference between their widths. Figure 2b shows the simulated spray combustion behavior of case 2, which was similar to that of case 1. The detailed flame propagation process was vividly represented, and it is important and meaningful for the systematic study of spray combustion characteristics. Therefore, in general, the numerical model used in this paper could greatly describe the detailed development process of spray flame and capture the important behaviors regardless of a minor difference in the spatial size.

Then, Figure 3 further compares the simulation results of the heat release rate (HRR) with the experimental data in case 1 and case 2. Neglecting the oscillations in the initial HRR due to the measurements, case 1 and case 2 had a similar HRR trace, which showed a typical diffusion combustion characteristic. For example, there was an initial delay where the HRR was low, then a premixed peak at around t = 0.5 ms due to the combustion of the fuel–air mixture accumulated during the ignition delay, and following this peak was the regular diffusion-regulated combustion starting at around t = 0.9 ms, with the diffusion peak appearing at around t = 1.75 ms. The simulated HRR in both cases showed qualitatively the same trend as in the experiments, with a slight mismatch in the HRR values. In both cases, the simulated premixed HRR peak came around 0.2 ms later than the experimental data peak, and the simulation results of the HRR during the premixed combustion were slightly smaller than in the experiments with a difference within 10%. After the premixed peak at t = 0.5 ms, the simulation results of HRR gradually exceeded those of the experimental data with a difference even over 10% until t = 2.3 ms. The maximum difference reached 60% at t = 0.8 ms for case l and 40% at t = 0.88 ms for case 2. The discrepancy mainly comes from two aspects. First is the grid setting, which could not completely reproduce the practical interaction between the aerosol and the turbulence and also the relative velocity between the liquid and the gas phase. However, these discrepancies were undoubtedly reasonable for a 3D CFD simulation to some extent, since the best grid settings are extremely difficult to adjust, and an overly complex grid setting brings a large computation cost. Another reason is that the heat transfer loss from the wall of the CVCC was neglected when simulating, so the simulated premixed peak and diffusion peak of the HRR were both higher than

those of the experimental data. Obviously, there was hardly any difference between the simulation results and the experimental data in the location of the diffusion HRR peak; meanwhile, the difference between the simulated HRR and the experimental one during the late burning gradually decreased to less than 10%. Therefore, regardless of the reasonable discrepancies between the simulation results and the experimental data, the calibrated 3D CFD model was reasonably and reliably used to investigate the detailed diesel spray combustion behavior.

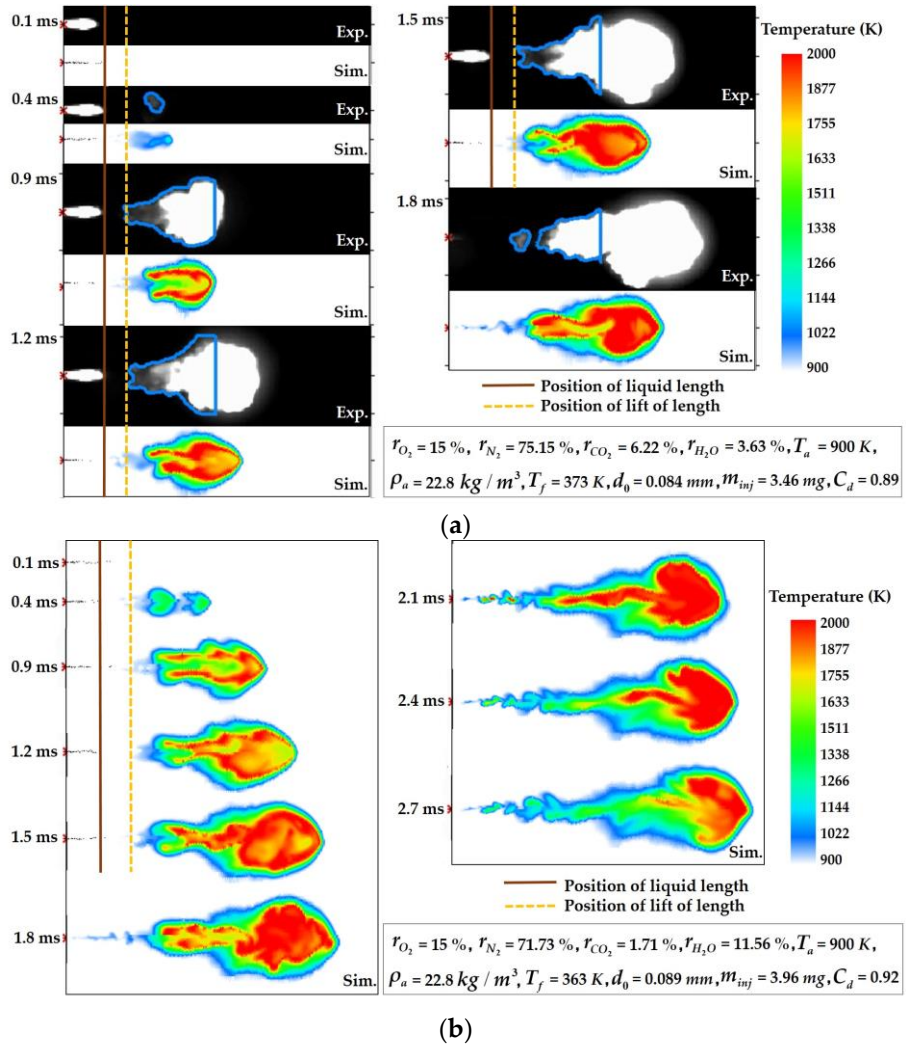

Figure 2. Evolution process of spray combustion flame in different cases: (**a**) case 1; (**b**) case 2.

3.2. Impact of Flexible Injection Rates

A multiple-injection strategy has a significant influence on improving the spray mixing characteristics and combustion characteristics. In our previous study [27], it was found that a multiple-injection strategy with a higher initial injection rate could greatly promote the spray mixing process. Continuing with the previous effort, this study further explored the influence of this positive advanced multiple-injection strategy on the spray combustion and emission behaviors. Three different multiple-injection strategies, including the high 2 rectangular injection rate shape (H2RECT), the low 2 rectangular injection rate shape (L2RECT), and the low 2 rectangular injection rate with a long dwell time shape (L2RECTLt) were selected. The H2RECT injection rate had a higher first injection rate than that of the L2RECT injection rate, in order to study the influence of the initial injection rate; the L2RECTLt injection rate had a longer dwell time than that of the L2RECT injection rate, in order to study the influence of the dwell time. Their injection parameters and injection rates are shown in Table 3 and Figure 4, respectively. The peak injection pressures

were set as 453 MPa in the case of H2RECT and 255 MPa in the cases of L2RECT and L2RECTLt, to better explore the spray combustion behavior under the ultrahigh injection pressure condition.

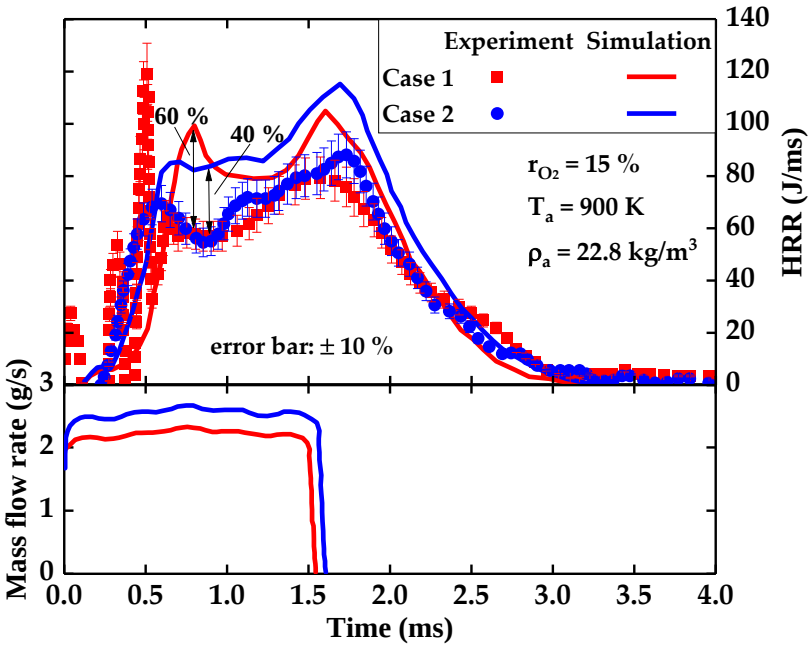

Figure 3. Comparison of simulation results of HRR and experimental data in different cases.

Table 3. Injection parameters of multiple-injection strategies.

Injection Rate Shape	1st Injection Duration (ms)	Dwell (ms)	2nd Injection Duration (ms)
H2RECT	0.70	0.15	0.75
L2RECT	0.80	0.15	0.80
L2RECTLt	0.80	0.30	0.80

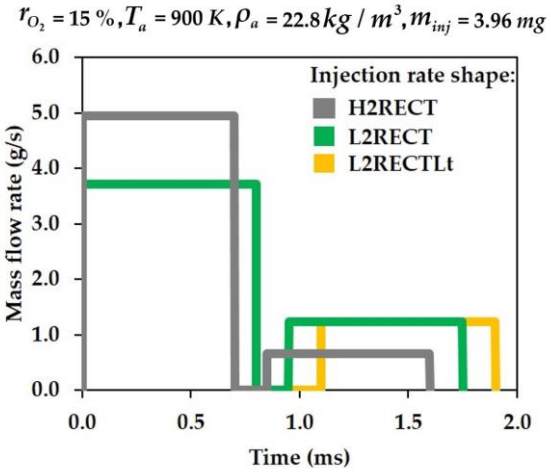

Figure 4. Injection rate shapes of various multiple-injection strategies.

Figure 5 shows the variations of the spray angle and spray profile in different multiple-injection strategies. Since H2RECT had a much larger first injection rate than L2RECT and L2RECTLt, its spray could obtain a higher axial penetrating momentum, contributing to a larger spray angle in the initial period and a longer spray penetration length. For example, at t = 0.7 ms, the spray penetration length of H2RECT was 12 mm longer than that of L2RECT and was 8 mm longer than that of L2RECTLt. After that, the difference gradually

decreased, and the spray penetration length of H2RECT was around 5 mm longer than that of L2RECT and was 7 mm longer than that of L2RECTLt at t = 1.9 ms. Meanwhile, the ultrahigh injection pressure also caused H2RECT to have a stronger turbulent mixing effect, which could be clearly reflected at the spray tip structure. Especially at t = 0.7 ms and t = 1.0 ms, the spray tip of H2RECT was circumferentially expanded nearly two times more than that of L2RECT and L2RECTLt, which greatly improved the fuel–air mixing effect of H2RECT. Compared with L2RECT, L2RECTLt had a larger dwell time between the first injection and second injection, which made the first spray have more time to interact with the ambient air and greatly enhanced the effect of the entrainment wave [16], so its spray angle after the end of the first injection was larger than that of L2RECT. Especially at t = 1.3 ms, the spray angle of L2RECTLt was 9 degrees larger than that of L2RECT, and the radial dimension of L2RECTLt approached two times that of L2RECT at around 30 mm downstream. However, due to the same peak pressure of the first injection in L2RECT and L2RECTLt, there was no big difference between their spray penetration length at each instant. Therefore, these results illustrated that the peak injection pressure had a significant influence on the spray axial penetration while the dwell time mainly affected the spray radial expansion.

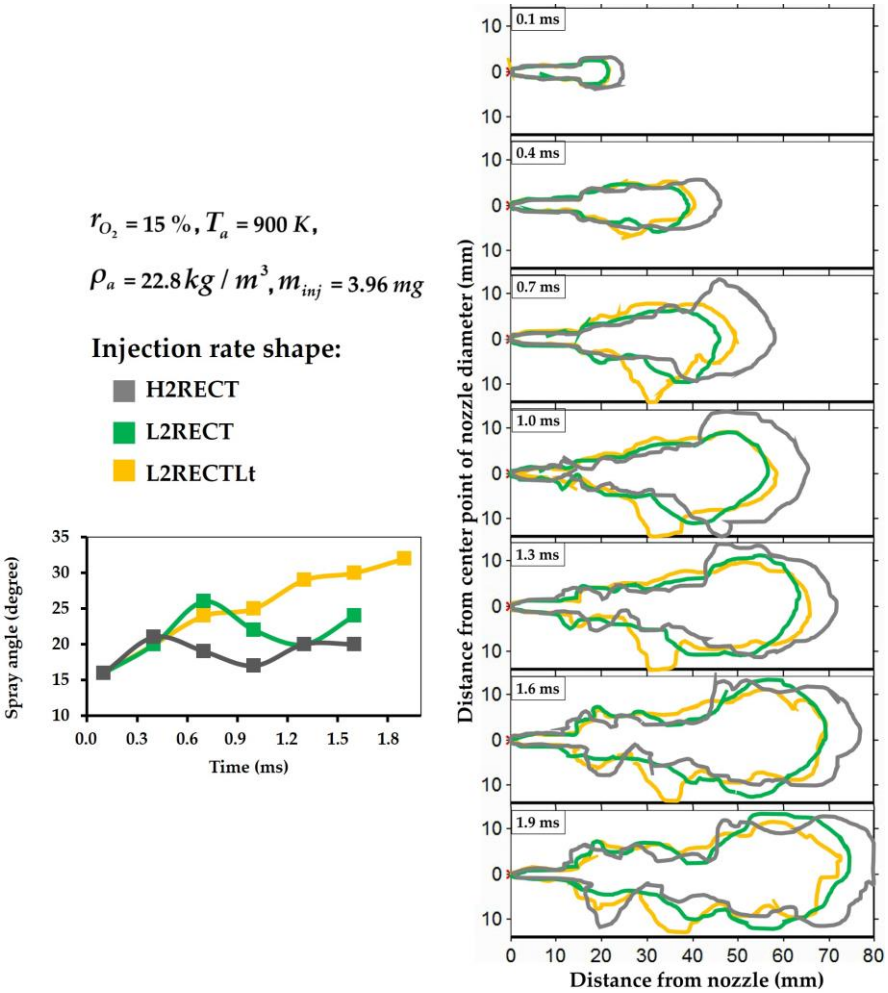

Figure 5. Variations of spray angle and spray boundaries in different multiple-injection strategies.

Figure 6 further shows the TKE history and the equivalence ratio distribution in different multiple-injection strategies. Obviously, because of the much higher peak injection pressure, the TKE of H2RECT was 20% larger than that of L2RECT and L2RECTLt from t = 0.1 ms to t = 0.8 ms, as shown in Figure 6a. At t = 1.6 ms, it can be found that there was a larger zone with a high TKE for H2RECT from 40 mm to 75 mm downstream. While at

t = 2.2 ms and t = 3.1 ms, H2RECT still kept a larger TKE level from 60 mm downstream to the spray tip compared with L2RECT and L2RECTLt. This also caused H2RECT to have a stronger vortex at the spray tip, especially at t = 0.7 ms; the downstream flow field was extremely stronger, contributing to a faster dilute equivalence ratio as shown in Figure 6b. It is obvious that the average equivalence ratio level of the area from 40 mm downstream to the spray tip in H2RECT was much lower than that of L2RECT and L2RECTLt until t = 3.1 ms. Meanwhile, there was always a strong flow field going through the whole spray plume in H2RECT, which was beneficial for the material transfer and fuel–air interaction. However, at the late stage of the spray development in L2RECT, the flow field mainly gathered in the spray tip region and left a relatively fuel-rich region in the upstream region, leading to a heterogeneous equivalence ratio distribution. Compared with L2RECT, L2RECTLt showed a larger overall TKE and a stronger vortex structure at the large scale, especially at t = 1.3 ms and t = 2.5 ms, which directly indicated that increasing the dwell time could greatly enhance the turbulence mixing effect. At t = 0.7 ms, the spray radial expansion of L2RECTLt was also increased, meaning a larger fuel–air interaction region. Undoubtedly, these positive effects greatly improved the further combustion behavior in the case of L2RECTLt.

In order to explore the influence of the aforementioned multiple-injection strategies on the combustion behavior, Figure 7 shows the variations of the combustion chamber pressure and the flame temperature in these cases. It is clear that the combustion chamber pressure in the case of H2RECT was higher than that of L2RECT and L2RECTLt from t = 0.6 ms to t = 2.2 ms and reached a maximum difference of 0.008 MPa at t = 1.2 ms. This was because the higher peak injection pressure of H2RECT greatly improved the aforementioned fuel–air mixing efficiency, contributing to more combustible fuel and more heat released in the initial period. From the temperature distribution in Figure 7, it can be seen that H2RECT appeared to have a snatchier flame structure due to the stronger turbulent mixing effect from the ultrahigh peak injection pressure. Especially in the zone of 30 mm downstream to 60 mm downstream in H2RECT, the flame shape was extremely irregular and many small flame vortexes were formed. Meanwhile, in that region, the overall temperature distribution of H2RECT was relatively homogeneous with a low temperature, which is extremely beneficial to lower the thermal load of the cylinder wall and reduce the productions of soot and NO_x in engineering applications. When comparing L2RECT and L2RECTLt, the flame of the latter was wider in the radial direction with a smaller high-temperature region at the spray tip, especially at t = 1.6 ms and t = 2.2 ms. This resulted from the enhanced turbulence mixing effect due to the increased dwell time.

To compare the combustion rate, Figure 8 shows the simulation results of the HRR in different multiple-injection strategies. The combustion characteristics in these three cases are similar to that in Figure 3, but due to the ultrahigh injection pressure in these three cases, the fuel–air mixing was greatly promoted, so the diffusion combustion stage after the premixed HRR peak was much shorter than that in Figure 3. Benefitting from the initial stronger turbulence mixing effect, H2RECT showed a shorter ignition delay, which decreased by 10% compared to that of L2RECT and L2RECTLt, while the latter two cases had a similar ignition delay due to the same first injection rate. Meanwhile, the ultrahigh peak injection pressure also brought more combustible fuel in the initial period for H2RECT, especially contributing to a much larger peak HRR, which was approximately 46.7% higher than that of L2RECT. However, since the second injection rate of H2RECT was lower, the HRR in the late burning stage of H2RECT became gradually smaller than the other two cases after t = 1.2 ms. In addition, it was obvious that L2RECTLt had an approximately 13.3% larger peak HRR than L2RECT, because L2RECTLt had a better turbulence mixing process due to the increased dwell time, as discussed above. Because of the same second injection rate in L2RECT and L2RECTLt, there was no big difference between their HRR in the late burning stage. However, comparatively speaking, increasing the first injection rate seemed to have a tremendous edge over increasing the dwell time in promoting

the combustion efficiency. It is absolutely a significant finding for guiding the design of injection and combustion strategies.

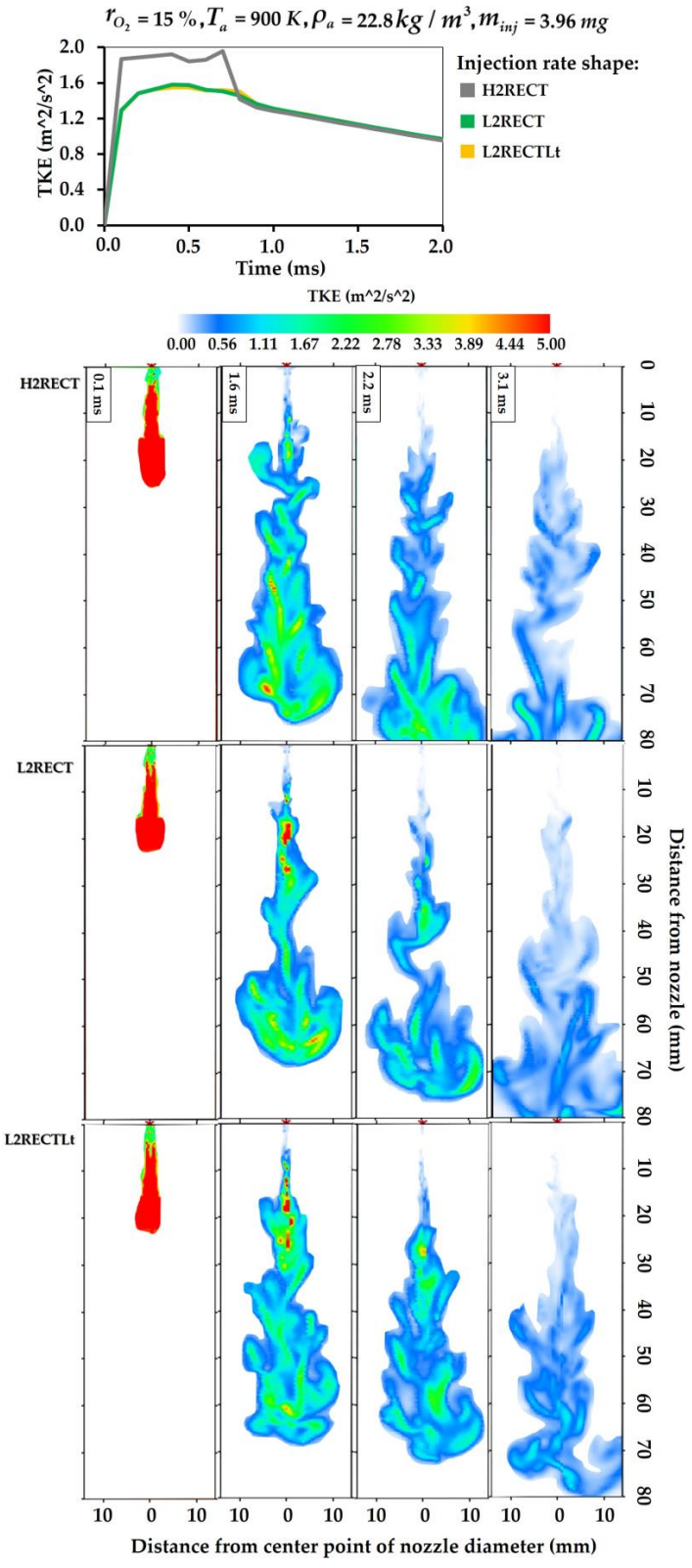

(**a**)

Figure 6. *Cont.*

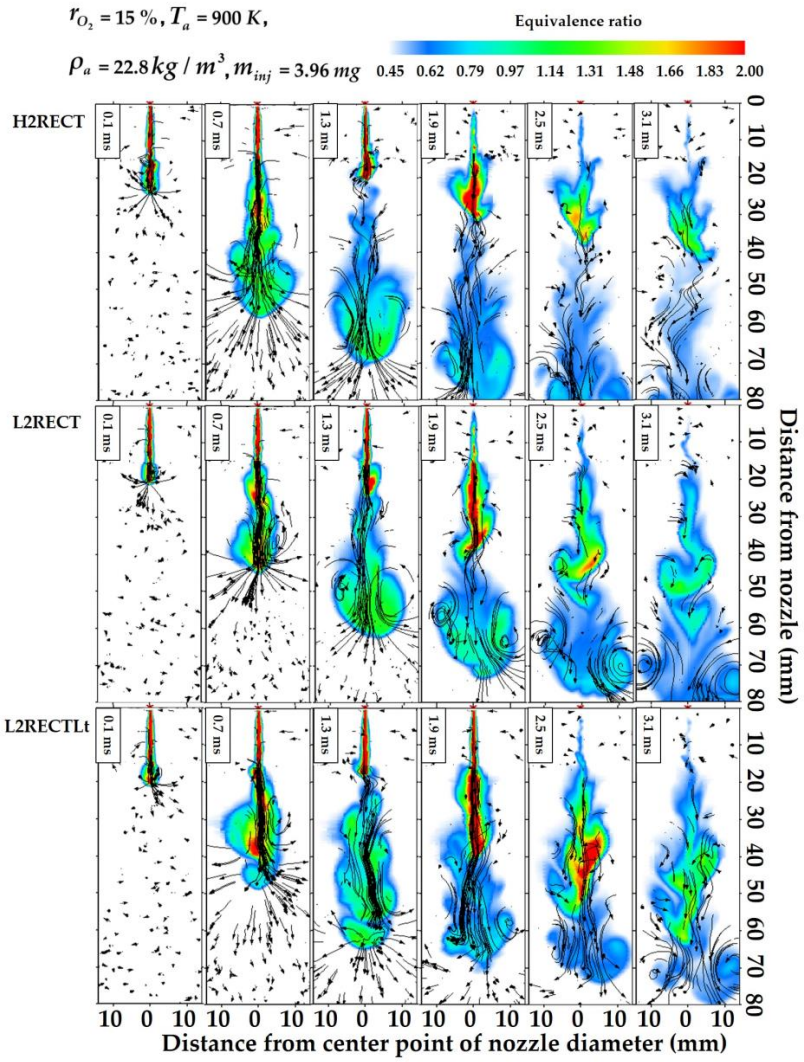

(**b**)

Figure 6. Spray characteristics distribution history in different multiple-injection strategies: (**a**) TKE; (**b**) equivalence ratio.

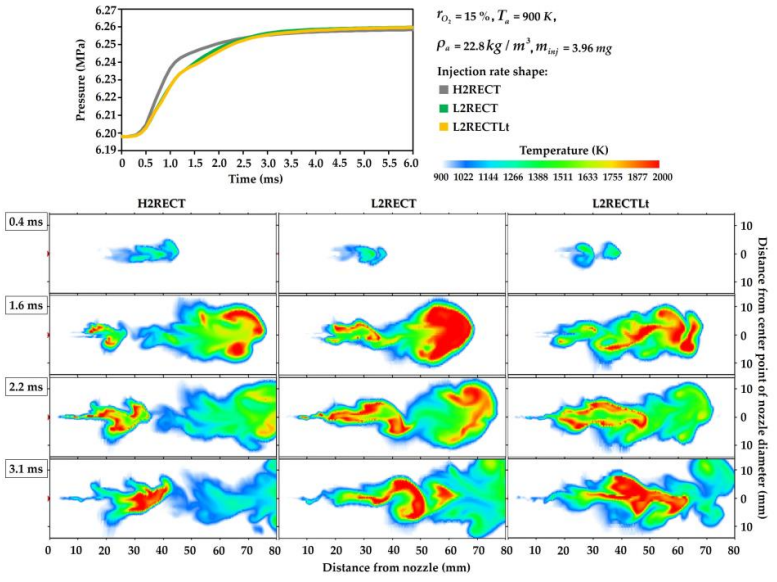

Figure 7. Variation of combustion chamber pressure and flame temperature.

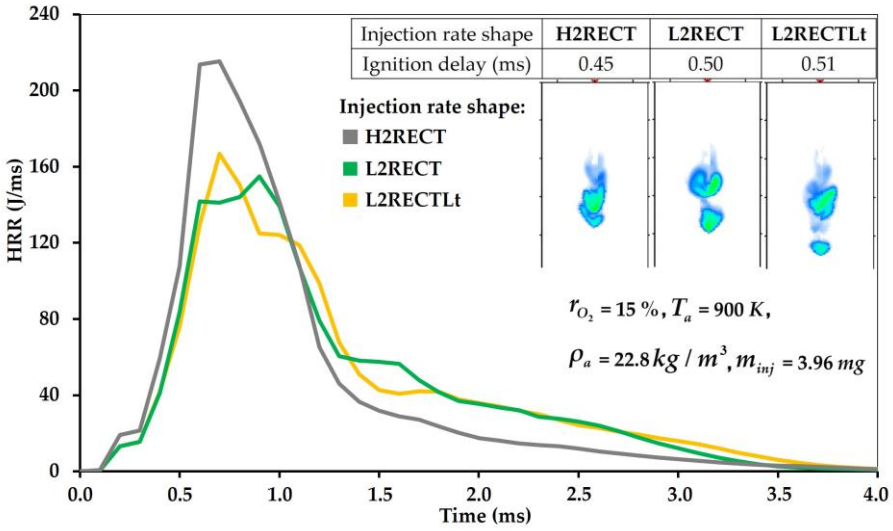

Figure 8. Variation of HRR in different multiple-injection strategies.

In addition to the mixing characteristics and the combustion characteristics, the emission characteristics is also a key factor to evaluate the potential of the flexible fuel injection strategy. Figure 9 shows the formation history of soot and NO_x emissions in different multiple-injection strategies. In Figure 9a, it can be found that H2RECT obtained a slightly higher soot amount and NO_x amount than that of L2RECT and L2RECTLt before t = 1.0 ms and t = 2.2 ms, respectively. This was because the higher peak injection pressure of H2RECT greatly promoted the premixed combustion as shown in Figure 8 and contributed to more combustible fuel and more heat released in the initial period, which provided a more favorable environment for soot and NO_x formation. Then, the amounts of soot and NO_x in H2RECT gradually became lower than that of L2RECT and L2RECTLt, and H2RECT obtained the lowest final amounts of soot and NO_x. Comparatively, the final soot amount of H2RECT was approximately 16.7% and 33.5% lower than that of L2RECT and L2RECTLt, respectively, while the final NO_x amount of H2RECT was approximately 31.4% and 20.0% lower than that of L2RECT and L2RECTLt, respectively. On the one hand, the late burning of H2RECT was not as strong as that of L2RECT and L2RECTLt due to the lower second injection rate, so H2RECT formed a lower amount of soot during this stage. On the other hand, the peak injection pressure of H2RECT greatly improved the spray's turbulent mixing process, leading to a homogeneous temperature distribution with a low temperature, such as the 30 mm to 60 mm downstream zone in Figure 7, which prevented the high-temperature combustion reaction, so the NO_x formation was greatly reduced. As shown in Figure 9b, it is obvious that the soot formation distribution and NO_x formation distribution got quickly diluted after t = 1.0 ms and t = 1.6 ms, respectively. Compared with L2RECT, L2RECTLt had a broader flame but with a relatively smaller high-temperature region such as that at t = 1.6 ms. Therefore, the final amount of soot formation was higher, but the final amount of NO_x formation was lower in the case of L2RECTLt. From the emission characteristics in different multiple-injection strategies, we found that increasing the first injection rate had the double advantages of reducing soot and NO_x simultaneously, while increasing the dwell time brought a compromise in emission reduction.

In summary, H2RECT was demonstrated to be the best injection pattern for enhancing the spray mixing, promoting the combustion efficiency and reducing the exhaust emissions simultaneously. It could give a valuable and significant guidance in practical engineering applications.

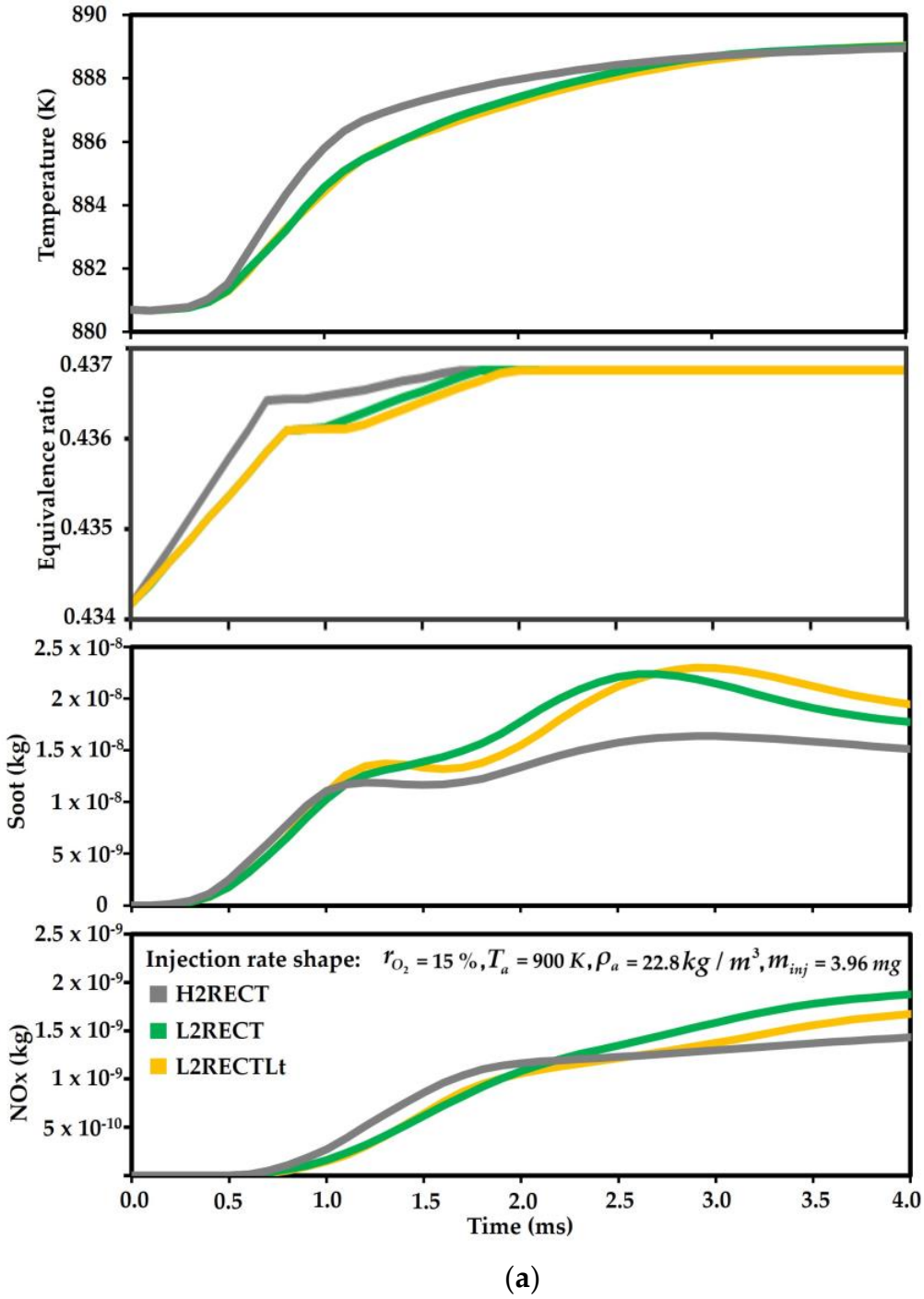

(**a**)

Figure 9. *Cont.*

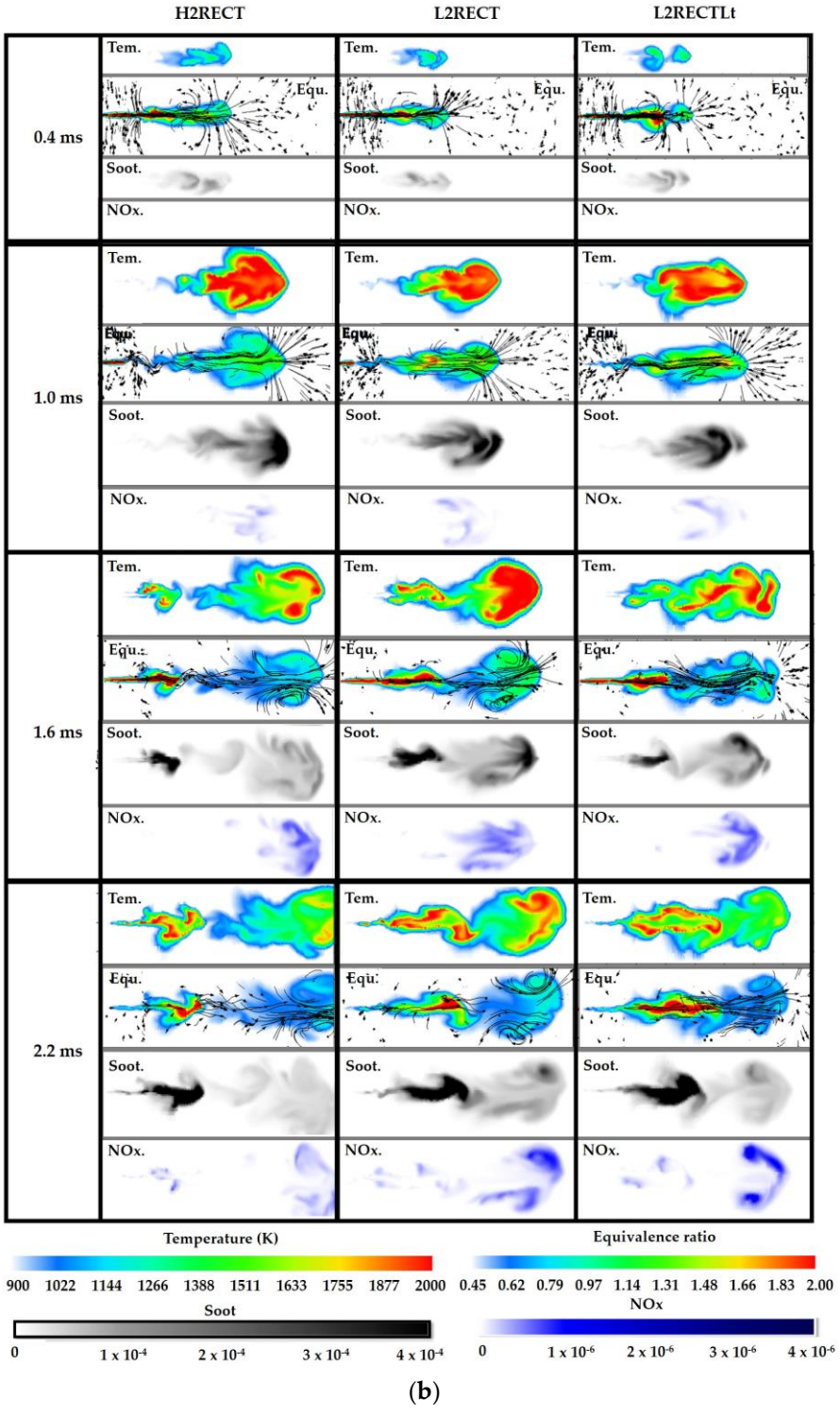

Figure 9. Formation history of soot and NO_x emissions in different multiple-injection strategies: (**a**) macroscopic variations; (**b**) microscopic distributions.

4. Conclusions

The CFD technique was used to investigate the combustion and emission characteristics of a diesel engine under a flexible fuel injection strategy with an ultrahigh injection pressure. The simulation was performed by coupling the LES model and the SAGE combustion model, with the model validated by experimental data. The processes of spray mixing, combustion flame propagation and exhaust emissions generation under differ-

ent multiple-injection strategies were deeply investigated. The obtained conclusions are as follows:

(1) The initial ultrahigh injection pressure had a significant influence on the spray axial penetration while the dwell time mainly affected the spray radial expansion.
(2) The H2RECT injection pattern obtained a 20% larger TKE than the L2RECT and the L2RECTLt injection patterns during the first injection due to the initial ultrahigh injection pressure. In the H2RECT injection pattern, the vortex at the spray tip and the downstream flow field were much stronger, contributing to a faster dilute equivalence ratio. There was always a strong flow field going through the whole spray plume in the H2RECT injection pattern, which was beneficial for the material transfer and fuel–air interaction.
(3) The H2RECT injection pattern showed an approximately 46.7% higher peak HRR than that of the L2RECT injection pattern because its ultrahigh peak injection pressure brought more combustible fuel in the initial period. The L2RECTLt injection pattern had an approximately 13.3% larger peak HRR than the L2RECT injection pattern due to the better turbulence mixing process from the increased dwell time. However, comparatively, increasing the first injection rate seemed to have a tremendous edge over increasing the dwell time for promoting the combustion efficiency.
(4) The final soot amount of H2RECT was approximately 16.7% and 33.5% lower than that of L2RECT and L2RECTLt, respectively, which was because the late burning of the H2RECT injection pattern was not as strong as that of the L2RECT and L2RECTLt injection patterns due to the lower second injection rate, contributing to a lower formation amount of soot for the H2RECT injection pattern during that stage.
(5) The final NO_x amount of H2RECT was approximately 31.4% and 20.0% lower than that of L2RECT and L2RECTLt, respectively. It was because the peak injection pressure of the H2RECT injection pattern greatly improved the spray turbulent mixing process, leading to a homogeneous temperature distribution with a low temperature, which prevented the high-temperature combustion reaction, so the NO_x formation was greatly reduced.

In general, this paper presented an optimal injection strategy for engineering applications to improve the engine efficiency and cope with the increasingly serious emission problems. However, facing the development of flexible fuel engines, the properties of the fuel itself are also important factors. Thus, the matching study of alternative fuels with flexible injection strategies is also needed in the next step.

Author Contributions: Conceptualization, Q.M., I.N. and L.L.; methodology, I.N. and L.L.; software, I.N. and Y.W.; validation, Q.M., I.N. and L.L.; formal analysis, Q.M.; investigation, I.N.; resources, L.L.; data curation, I.N.; writing—original draft preparation, Q.M.; writing—review and editing, Q.M. and L.L.; visualization, Y.W.; supervision, X.M.; project administration, L.L. and X.M.; funding acquisition, L.L. All authors have read and agreed to the published version of the manuscript.

Funding: This research was funded by "Ye Qisun" Science Foundation of National Natural Science Foundation of China, grant number U2241262, Research of Controllable Combustion Technology in Marine Diesel Engine from National Key R&D Program of China, Ministry of Science and Technology, grant number 2017YFE0116400 and Natural Science Foundation for Distinguished Young Scholars of Heilongjiang Province, grant number JQ2020E005.

Institutional Review Board Statement: Not applicable.

Informed Consent Statement: Not applicable.

Data Availability Statement: Not applicable.

Conflicts of Interest: The authors declare no conflict of interest.

Nomenclature

3D	three-dimensional
A_r	factor of pre-exponential
B_1	KH model constant
b_r	temperature exponent
CFD	computational fluid dynamics
CVCC	constant volume combustion chamber
C_τ	correction factor in RT model
$\overline{c}_{p,m}$	molar constant-pressure specific heat of species m
D	mass diffusivity
ECN	Engine Combustion Network
EGR	exhaust gas recirculation
E_r	activation energy
H	enthalpy
H2RECT	high 2 rectangular injection rate shape
HRR	heat release rate
h_s	sensible enthalpy
$\overline{h}_m$	molar specific enthalpy of species m
$\overline{h}_t$	total enthalpy
KH	Kelvin–Helmholtz
K_{cr}	equilibrium coefficient
K_{pr}	equilibrium constant
k_{fr}	forward rate coefficient
k_{rr}	reverse rate coefficient
L2RECT	low 2 rectangular injection rate shape
L2RECTLt	low 2 rectangular injection rate with long dwell time shape
LES	large-eddy simulation
LTC	low temperature combustion
NTC	no time counter
p	pressure
PCCI	premixed charge combustion ignition
PISO	Pressure-Implicit with Splitting of Operators
p_{atm}	atmospheric pressure
r	radius of the initial droplets
R	constant of gas
R_u	constant of universal gas
S	entropy
$\overline{S}_h$	energy source term
$\overline{S}_{u_i}$	momentum source term
$\overline{S}_{Y_k}$	species source term
$\overline{S}_\rho$	mass source term
RT	Rayleigh–Taylor
TKE	turbulence kinetic energy
u_i	velocity component in x_i direction
URANS	unsteady Reynolds averaged Navier–Stokes
Y_k	chemical species k mass fraction
ρ	density
μ	viscosity diffusion rate
Ω_{KH}	disruptive growth rate in KH model
Ω_{RT}	growth rate in RT model
Λ_{KH}	wavelength in KH model
Λ_{RT}	wavelength in RT model
τ_{KH}	KH breakup time
τ_{RT}	RT breakup time
$\overline{\tau}_{ij}$	viscous stress tensor

References

1. Nayak, S.K.; Nižetić, S.; Pham, V.V.; Huang, Z.; Ölçer, A.I.; Bui, V.G.; Wattanavichien, K.; Hoang, A.T. Influence of injection timing on performance and combustion characteristics of compression ignition engine working on quaternary blends of diesel fuel, mixed biodiesel, and t-butyl peroxide. *J. Clean. Prod.* **2022**, *333*, 130160. [CrossRef]
2. Hoang, A.T.; Pham, V.V. A review on fuels used for marine diesel engines. *J. Mech. Eng. Res. Dev. (JMERD)* **2018**, *41*, 22–32. [CrossRef]
3. Bui, V.G.; Tu Bui, T.M.; Hoang, A.T.; Nižetic, S.; Nguyen Thi, T.X.; Vo, A.V. Hydrogen-enriched biogas premixed charge combustion and emissions in direct injection and indirect injection diesel dual fueled engines: A comparative study. *J. Energy Resour. Technol.—Trans. ASME* **2021**, *143*, 120907. [CrossRef]
4. Iqbal, M.; Wang, T.; Li, G.; Li, S.; Hu, G.; Yang, T.; Gu, F.; Al-Nehari, M. Development and Validation of a Vibration-Based Virtual Sensor for Real-Time Monitoring NO_x Emissions of a Diesel Engine. *Machines* **2022**, *10*, 594. [CrossRef]
5. Gürbüz, H.; Demirtürk, S.; Akçay, İ.H.; Akçay, H. Effect of port injection of ethanol on engine performance, exhaust emissions and environmental factors in a dual-fuel diesel engine. *Energy Environ.* **2021**, *32*, 784–802. [CrossRef]
6. United States Environmental Protection Agency. Available online: https://www.epa.gov/regulations-emissions-vehicles-and-engines (accessed on 17 March 2022).
7. Jo, S.; Cha, J.; Park, S. Exhaust emission characteristics of stoichiometric combustion applying to diesel particulate filter (DPF) and three-way catalytic converter(TWC). *Energy* **2022**, *254*, 124196. [CrossRef]
8. Bobi, S.; Kashif, M.; Laoonual, Y. Combustion and emission control strategies for partially-premixed charge compression ignition engines: A review. *Fuel* **2022**, *310*, 122272. [CrossRef]
9. Batool, S.; Naber, J.D.; Shahbakhti, M. Multi-mode Low Temperature Combustion (LTC) and Mode Switching Control. In *Advanced Combustion for Sustainable Transport*; Agarwal, A.K., Martínez, A.G., Kalwar, A., Valera, H., Eds.; Energy, Environment, and Sustainability; Springer: Singapore, 2022; pp. 43–93, ISBN 9789811684173.
10. Chen, D.; Wang, T.; Yang, T.; Li, G.; Chen, Y.; Qiao, T. Effects of EGR combined with DOC on emission characteristics of a two-stage injected Fischer-Tropsch diesel/methanol dual-fuel engine. *Fuel* **2022**, *329*, 125451. [CrossRef]
11. Payri, R.; Gimeno, J.; Viera, J.P.; Plazas, A.H. Needle lift profile influence on the vapor phase penetration for a prototype diesel direct acting piezoelectric injector. *Fuel* **2013**, *113*, 257–265. [CrossRef]
12. Macian, V.; Payri, R.; Ruiz, S.; Bardi, M.; Plazas, A.H. Experimental study of the relationship between injection rate shape and Diesel ignition using a novel piezo-actuated direct-acting injector. *Appl. Energy* **2014**, *118*, 100–113. [CrossRef]
13. Aalam, C.S.; Saravanan, C.G.; Anand, B.P. Impact of high fuel injection pressure on the characteristics of CRDI diesel engine powered by mahua methyl ester blend. *Appl. Therm. Eng.* **2016**, *106*, 702–711. [CrossRef]
14. Nishida, K.; Zhu, J.; Leng, X.; He, Z. Effects of micro-hole nozzle and ultra-high injection pressure on air entrainment, liquid penetration, flame lift-off and soot formation of diesel spray flame. *Int. J. Engine Res.* **2017**, *18*, 51–65. [CrossRef]
15. Vera-Tudela, W.; Haefeli, R.; Barro, C.; Schneider, B.; Boulouchos, K. An experimental study of a very high-pressure diesel injector (up to 5000 bar) by means of optical diagnostics. *Fuel* **2020**, *275*, 117933. [CrossRef]
16. Naruemon, I.; Liu, L.; Mei, Q.; Ma, X. Investigation on an injection strategy optimization for diesel engines using a one-dimensional spray model. *Energies* **2019**, *12*, 4221. [CrossRef]
17. Naruemon, I.; Liu, L.; Liu, D.; Ma, X.; Nishida, K. An analysis on the effects of the fuel injection rate shape of the diesel spray mixing process using a numerical simulation. *Appl. Sci.* **2020**, *10*, 4983. [CrossRef]
18. Boggavarapu, P.; Singh, S. *Computational Study of Injection Rate-Shaping for Emissions Control in Diesel Engines*; SAE Technical Paper 2011-26-0081; SAE International: Warrendale, PA, USA, 2011. [CrossRef]
19. Ramirez, A.I.; Som, S.; Rutter, T.P.; Longman, D.E.; Aggarwal, S.K. Investigation of the Effects of Rate of Injection on Combustion Phasing and Emission Characteristics: Experimental and Numerical Study. In Proceedings of the Central States Section of the Combustion Institute Spring Technical Meeting, Dayton, OH, USA, 23–24 April 2012.
20. Mohan, B.; Yang, W.; Yu, W.; Tay, K.L.; Chou, S.K. Numerical investigation on the effects of injection rate shaping on combustion and emission characteristics of biodiesel fueled CI engine. *Appl. Energy* **2015**, *160*, 737–745. [CrossRef]
21. Tay, K.L.; Yang, W.; Zhao, F.; Yu, W.; Mohan, B. Effects of triangular and ramp injection rate-shapes on the performance and emissions of a kerosene-diesel fueled direct injection compression ignition engine: A numerical study. *Appl. Therm. Eng.* **2017**, *110*, 1401–1410. [CrossRef]
22. Skeen, S.; Manin, J.; Pickett, L.M. Visualization of Ignition Processes in High-Pressure Sprays with Multiple Injections of n-Dodecane. *SAE Int. J. Engines* **2015**, *8*, 696–715. [CrossRef]
23. Bolla, M.; Chishty, M.A.; Hawkes, E.R.; Kook, S. Modeling combustion under engine combustion network Spray A conditions with multiple injections using the transported probability density function method. *Int. J. Engine Res.* **2017**, *18*, 6–14. [CrossRef]
24. Cung, K.; Moiz, A.; Johnson, J.; Lee, S.Y.; Kweon, C.B.; Montanaro, A. Spray-combustion interaction mechanism of multiple-injection under diesel engine conditions. *Proc. Combust. Inst.* **2015**, *35*, 3061–3068. [CrossRef]
25. Moiz, A.A.; Ameen, M.M.; Lee, S.Y.; Som, S. Study of soot production for double injections of n-dodecane in CI engine-like conditions. *Combust. Flame* **2016**, *173*, 123–131. [CrossRef]
26. Zheng, Z.; Yue, L.; Liu, H.; Zhu, Y.; Zhong, X.; Yao, M. Effect of two-stage injection on combustion and emissions under high EGR rate on a diesel engine by fueling blends of diesel/gasoline, diesel/n-butanol, diesel/gasoline/n-butanol and pure diesel. *Energy Convers. Manag.* **2015**, *90*, 1–11. [CrossRef]

27. Naruemon, I.; Liu, L.; Mei, Q.; Wu, Y.; Ma, X.; Nishida, K. Investigating the effect of split injection with different injection patterns on diesel spray mixing. *Front. Energy Res.* **2022**, *10*, 933591. [CrossRef]
28. Rostampour, A.; Shojaeefard, M.H.; Molaeimanesh, G.R. A comprehensive investigation of RANS and LES turbulence models for diesel spray modeling via experimental diesel schlieren imaging. *Proc. Inst. Mech. Eng. Part C J. Mech. Eng. Sci.* **2022**, *236*, 8321–8337. [CrossRef]
29. Nemati, A.; Ong, J.C.; Walther, J.H. CFD analysis of combustion and emission formation using URANS and LES under large two-stroke marine engine-like conditions. *Appl. Therm. Eng.* **2022**, *216*, 119037. [CrossRef]
30. Salehi, F.; Ghiji, M.; Chen, L. Large eddy simulation of high pressure spray with the focus on injection pressure. *Int. J. Heat Fluid Flow* **2020**, *82*, 108551. [CrossRef]
31. Wen, X.; Gierth, S.; Rieth, M.; Chen, J.H.; Hasse, C. Large-eddy simulation of a multi-injection flame in a diesel engine environment using an unsteady flamelet/progress variable approach. *Phys. Fluids* **2021**, *33*, 105107. [CrossRef]
32. Senecal, P.K.; Pomraning, E.; Richards, K.J.; Briggs, T.E.; Choi, C.Y.; McDavid, R.M.; Patterson, M.A. *Multi-Dimensional Modeling of Direct-Injection Diesel Spray Liquid Length and Flame Lift-Off Length Using CFD and Parallel Detailed Chemistry*; SAE Technical Paper 2003-01-1043; SAE International: Warrendale, PA, USA, 2003. [CrossRef]
33. Sun, X.; Liang, X.; Shu, G.; Wang, Y.; Wang, Y.; Yu, H. Effect of different combustion models and alternative fuels on two-stroke marine diesel engine performance. *Appl. Therm. Eng.* **2017**, *115*, 597–606. [CrossRef]
34. Gong, C.; Jangi, M.; Bai, X.S. Large eddy simulation of n-Dodecane spray combustion in a high pressure combustion vessel. *Appl. Energy* **2014**, *136*, 373–381. [CrossRef]
35. Engine Combustion Network. Available online: http://www.sandia.gov/ecn (accessed on 17 March 2022).
36. Som, S.; Aggarwal, S.K. Effects of primary breakup modeling on spray and combustion characteristics of compression ignition engines. *Combust. Flame* **2010**, *157*, 1179–1193. [CrossRef]
37. Mehl, M.; Pitz, W.J.; Westbrook, C.K.; Curran, H.J. Kinetic modeling of gasoline surrogate components and mixtures under engine conditions. *Proc. Combust. Inst.* **2011**, *33*, 193–200. [CrossRef]